Vietnam Journal of Catalysis and Adsorption
Tạp chí xúc tác và hấp phụ Việt Nam

http://chemeng.hust.edu.vn/jca/

Study on the synthesis and properties of porous cadmium zeolitic imidazolate framework for environmental treatment

Ninh Duc Ha, La Duc Duong, and Nguyen Thi Hoai Phuong*

Institute of Chemistry and Materials, Hanoi, VIETNAM
**Email: hoaiphuong1978@gmail.com*

-Hội thảo quốc tế về Khoa học và Kỹ thuật Phân tách tiên tiến lần thứ hai (CASSE 2022)-

ARTICLE INFO

Received: 02/12/2022
Accepted: 15/3/2023
Published: 30/6/2023

Keywords:

cadmium imidazolate framework; adsorption capacity; metal-organic frameworks; environment treatment

ABSTRACT

In this study, cadmium imidazolate frameworks were synthesized by a solvothermal method from cadmium acetate and 2-methylimidazole in an ethanol/methanol mixture. The $Cd(Im)_2$ processed at 150 °C after 8 hours with the mixture of solvents has high crystallinity. The appearance of the absorption band at 407.73 cm^{-1} shows a link formation of Cd (II) and N within HIm's molecule. Cadmium imidazolate only formats zeolite crystal, the network fibers were potent, and the pores were alike. The dimension of pores is approximately 200 nm. The XRD diagram shows that the $Cd(Im)_2$ has high crystallinity. The $Cd(Im)_2$ phase is obvious from reflections at 7°, 10°, 12°, 14°, 15,6° and 17°. The surface area of $Cd(Im)_2$ was 662.894 m^2/g or 858.389 m^2/g with BET or Langmuir calculations, respectively. The maximum adsorption capacity of Cd-ZIF-8 for the RhB is 64.52 $mg.g^{-1}$, and the adsorption data were fitted well with a pseudo-second-order model.

Introduction

Manufactured dyes are notably troublesome chemical toxins. The industrial wastes of these dyes are exceedingly noxious to aerobic and aquatic life and can cause compounds that show carcinogenic, mutagenic, and neurotoxic effects [1, 2]. Moreover, they can expressly preclude light penetration and inhibit photosynthesis in aquatic plants [3]. The unsuitable discarding of an enormous quantity of these deleterious dyes not only results in remarkable environmental pollution but also in the loss of considerable expenditures that make the coloring industry one of the most polluting industries on the globe [4]. Rhodamine B (RhB) is a conventional organic dye that is universally used in industries because of its low cost. Even though RhB has many utilities in many industrial progressions, it is tremendously toxic and deleterious to the environment and human health, even at a low concentration of less than one ppm. It is essential to diminish RhB to an allowable concentration before throwing it into the environment [5].

A branch of porous metal-organic frameworks (MOFs), zeolitic imidazolate frameworks (ZIFs), have an individual bonding angle of 145° between the metal and the imidazolate linker (M-Im-M angle), which imitates the Si-O-Si angle of zeolites as first published in 2006 [6, 7]. These physicochemical properties make ZIFs outstanding adsorbents for apprehending toxins and gases ranging from small to large toxic molecules in water [7-9]. On this subject, ZIF-8, which has a high surface area, is among the most routinely researched ZIF materials. In ZIF-8, tetrahedrally coordinated zinc ions are linked by 2-methylimidazole (2-mIm) through its nitrogen atoms. The solidity of these porous crystals

https://doi.org/10.51316/jca.2023.033

in water makes them highly engaging materials for reduplicated adsorptive elimination in aqueous media [10]. Not long ago, it was published that a multiplicity of modified and unmodified ZIFs materials were successfully used as adsorbents for the degeneration of heavy metal ions and organic pollutants, such as dyes from wastewater [11-13]. Many researchers have reported the effectiveness of ZIF-8 in the elimination of organic dyes such as rhodamine 6G, triiodide, and methylene blue as well as benzotriazoles and phthalic acid, As(III), etc. [14-16]. For example, Chin and Anh Tran reported that nanosized ZIF-8 presents appreciable prospect for the adsorption and photodegradation of Rhodamine B [14, 17], while it indicated a low adsorption capacity for methyl orange [18-20].

Recently, zeolitic imidazolate frameworks (ZIFs) have attracted extensive research interest due to their potential applications in removing pollutants from wastewater. The Cd- zeolitic-imidazolate framework (Cd-ZIF-8) was published with the results of its adsorption to remove methyl orange (MO) at different operating conditions. The maximum MO adsorption capacity of Cd-ZIF-8 was 145.41 mg g-1 and the material has good stability after the adsorption with no release of Cd ions over a wide pH range [12].

The Cd-ZIF was also utilized for the ultrasound-assisted removal of malachite green (MG) dye. The experimental maximum adsorption capacity of MG onto Cd-ZIF was 3324.17 mg/g at 25 °C [21]. In this study, we report on the preparation, characterization, and properties of Cd-based MOFs with the 2-methylimidazole (MeIM) organic linker and investigate their adsorption capacity for Rhodamine B (RhB).

Experimental

Chemicals

Cadmium acetate dehydrate (98%), 2-methylimidazole (98%), methanol (97%), and ethanol (98%) were purchased from Xilong Chemical Company, China.

Synthesis of Cd-ZIF-8

A mixture of 0.267 g cadmium acetate dehydrate and 0.410 g 2-methylimidazole dissolved in a 15 mL mixture of ethanol/methanol (v/v: 1/1) was put into a 20 mL Teflon autoclave. The initial substance mixture was heated at various temperatures for 8 hours and then cooled to room temperature. After segregation by filtering, powder crystals were purified with ethanol (3 x 10 mL) and evacuated in vacuum at room temperature.

Characterization techniques

The infrared (IR) spectra of the material samples were recorded using a FT-IR spectrometer (Brucker, Germany) in the range of 400-4000 cm^{-1}. Scanning electron microscopy (SEM; Hitachi S-4600, Japan) was used for imaging the surface and morphologies of materials. Powder X-ray diffraction (XRD) patterns were measured using an X'Pert Pro diffractometer (Jeol, Japan) with CuK_α radiation (15 mA and 40 kV) at a scan rate of $2°.min^{-1}$ with a step size of 0.02°. The specific surface area values of $Cd(Im)_2$ were calculated by the Brunauer Emmett Teller (BET) method and the Langmuir method using the nitrogen adsorption isotherm.

Adsorption experiments

A series of experiments were conducted at room temperature. Different initial concentrations of RhB (20, 40, 60, 80, and 100 mg/L) were used to study the effect of contact time. This was done by mixing an amount of Cd-ZIF-8 with V = 100 mL of RhB solution at different pHs in the dark. The mass of adsorbent was added 0.1 g to V = 100 mL of RhB solution with initial concentration of C_0 = 20 mg/L and a self-generated pH (~ 7). The pH of the solution was controlled by adding HCl (0.1 M) and NaOH (0.1 M). At the reserved times, the remaining RhB solution was analyzed, and its residual concentration at equilibration time t (min), (C_e, in mg/L) was determined by a UV-vis photo-spectrometer (DV-8200 Drawell) at 552 nm.

C_0 and C_e values were used to estimate the amount of RhB adsorbed on the Cd-ZIF-8, at each equilibrium, q_e (mg/g) determining the following equation:

$$q_e = \frac{C_0 - C_e}{m_{Cd-ZIF}} \times V_{RhB}$$

where $m_{Cd\text{-}ZIF}$ is the Cd-ZIF-8 mass (g) and V_{RhB} is the volume of the RhB solution (L).

Different equilibrium isotherms and adsorption kinetic models were used to study the adsorption process. The linear curve fitting method in Excel software was employed to fit kinetic and isotherm models to the experimental data. To assure the sureness of results, each investigation was performed three times and averaged.

Both of the Langmuir and Freundlich models were used in this study to describe the adsorption equilibrium:

https://doi.org/10.51316/jca.2023.033

Langmuir: $\frac{C_e}{q_e} = \frac{1}{q_m} C_e + \frac{1}{K_L.q_m}$

Freundlich: $lnq_e = lnK_F + \frac{1}{n} lnC_e$

Where, q_e is the adsorption capacity at equilibrium ($mg.g^{-1}$), q_m is the maximum adsorption capacity of the adsorbent ($mg.g^{-1}$), K_L is Langmuir constant; C_e is the adsorbate concentration at equilibrium ($mg.m^{-3}$). K_F and n are model constants, K_F is related to the adsorption affinity of the adsorbent, and n indicates the adsorption process's support.

The adsorption kinetics of RhB were explored based on two models: pseudo-first-order and pseudo-second-order. The kinetic rate constants were calculated, respectively.

- The pseudo-first-order equation can be expressed as follows:

$$\ln(q_m - q_t) = lnq_m - k_1 \times \frac{t}{2.303}$$

where q_t and q_m are the adsorbed amounts ($mg.g^{-1}$) at time t (min), and at equilibrium, k1 (min^{-1}) is the corresponding adsorption rate constant.

- The pseudo-second-order model, as shown below, has been applied broadly for solute adsorption and catalysis reactions in liquid conditions:

$$\frac{t}{q_t} = \frac{1}{k_2 \times q_e^2} + \frac{t}{q_e}$$

where q_t and q_e are the adsorbed amounts ($mg.g^{-1}$) at time t (min) and at equilibrium, k_2 ($g.mg^{-1}.min^{-1}$) is the corresponding rate constant.

To explore the reusability of the prepared Cd-ZIF-8 after adsorption, the adsorbent was de-adsorbed through repeated washing with ethanol and then completely dried before next testing cycles. Five cycles were done, and the removal efficiency was determined by the UV-Vis spectrum. The removal performances were calculated according to the following formula:

$$H(\%) = \frac{(C_0 - C_n)}{C_0} \times 100$$

where C_0 (mg/L) is the initial concentration of the Rhodamine B solution, and C_n (mg/L) is the concentration of the dye solution after absorption at cycle n.

Results and discussion

Characterization of Cd-ZIF-8

The coordination mode between the ligands and the metal ion link was determined by analyzing the FT-IR spectra of the two ligands and Cd-ZIF-8. Figure 1 displays the IR spectra of the ligand (HIm) and its Cd(II) complex ($Cd(Im)_2$).

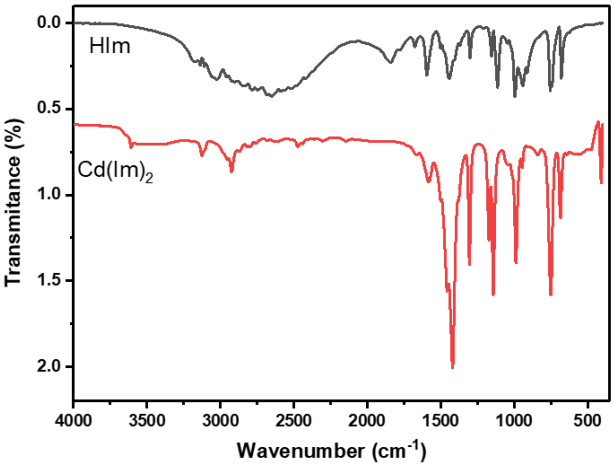

Figure 1: IR spectrum of 2-methylimidazole and Cadmium Imidazolate

In the IR spectra of 2-methylimidazole (Fig 1a), the broad absorption centered at 3608.07 cm^{-1} exhibits the -OH stretching vibration of the coordination water molecule. The absence of the expected absorption bands at 2653.27 cm^{-1} and 2517.46 cm^{-1} for the hydro bond internal molecule and at 1675 cm^{-1} and 1502.23 cm^{-1} for the protonated amine groups indicates the complete deprotonation of HIm ligand. In the complex, a new band is seen in the 407.73 cm^{-1}, which is probably due to the formation of the weak band observed in the < 500 cm^{-1} range, which is attributed to ν_{M-N} [12]. It shows the link formation of Cd (II) and N within HIm's molecule. This thing leads to the loss of the hydro bond internal molecule between HIms to the formation of $Cd(Im)_2$ following the below equation:

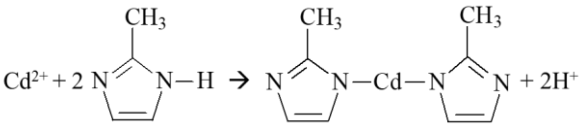

Along with the starting agents' ratio and solvent, the reaction temperature also strongly influences the formation of the framework structure. The SEM image of the prepared cadmium imidazolate shown in Figure 2 is the morphology of $Cd(Im)_2$ completed at different temperatures during the same 8-h reaction time. SEM images show that the reaction temperatures of 130 °C and 140 °C produce amorphous materials. Cadmium imidazoate shows zeolite crystal form at 150 °C. After 8 hours at 150 °C, the network fiber shape is precise, and the pores are uniform with a pore size of about 200 nm. But when the reaction occurs at 160 °C, $Cd(Im)_2$ forms an amorphous form, tends to cluster and close crystal arrangements, and does not create a hollow frame. This result shows that the porous framework structure can only form at a specific temperature.

https://doi.org/10.51316/jca.2023.033

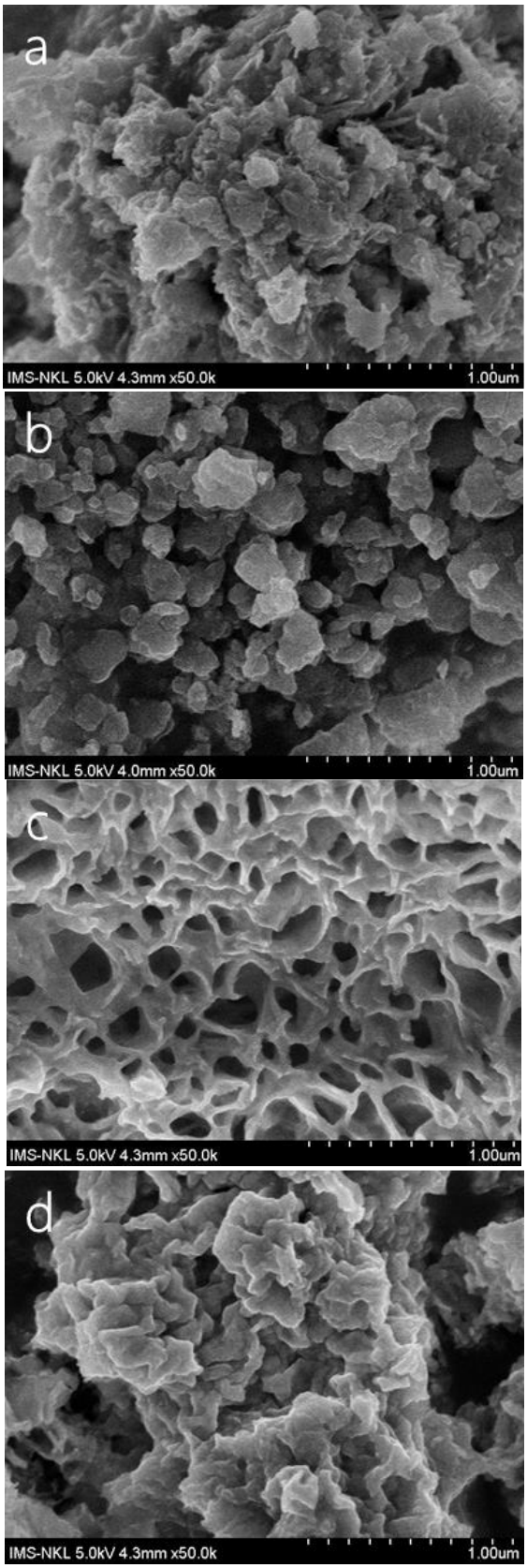

Figure 2: SEM image of $Cd(Im)_2$ prepared with different temperatures: 130°C (a); 140°C (b); 150°C (c); 160°C (d)

The crystal phase structure of $Cd(Im)_2$ determined using powder X-ray diffraction technique. The XRD patterns shown in Figure 3 are the phases of the $Cd(Im)_2$ prepared for different reaction conditions.

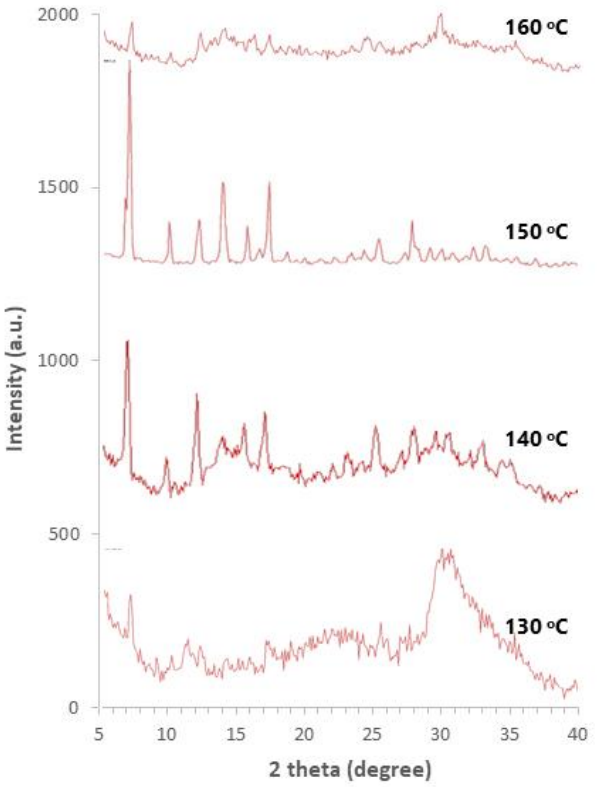

Figure 3: The XRD patterns of the $Cd(Im)_2$ prepared for different temperatures: 130°C (a); 140°C (b); 150°C (c); 160°C (d)

The crystal structure of $Cd(Im)_2$ is a complex mixture of variations in bond lengths and angles. Crystals are formed differently at each temperature. Although there is crystal formation at low reaction temperatures (130°C and 140°C), it is not obvious. On the XRD pattern of these samples, the appearance of peaks less than 10° is typical for the metal-organic framework with very low intensity. The XRD pattern of $Cd(Im)_2$ was prepared at 150°C after 8 hours with a high crystallinity ethanol/methanol mixed solvent (Figure 3c). The $Cd(Im)_2$ phase is clearly shown through reflections at 7 °, 10 °, 12 °, 14 °, 15.6 ° and 17 ° [22]. However, the crystal exhibits structural destruction with increasing reaction temperatures, for example, 160°C. Feature peaks in its XRD pattern disappear or have low intensity. According to the results of the study on a newly designed multi-carboxylate imidazole ligand [23], the framework of $Cd(Im)_2$ material forms networks with polymer-like structured voids. Specifically, every three cadmium atoms bond together through carboxylate ligands to form a heptagonal prism coordinated with two imidazole rings. This framework is only formed at a specific temperature, corresponding to the synthesis

condition of Cd(Im)2 framework material at 150°C. Meanwhile, at lower temperatures (130°C and 140°C), the formation of $Cd(Im)_2$ compound is in the form of a salt of cadmium metal and benzene carboxylate acid. As for the thermodynamics, at 150°C, the new equilibration variation reaches a value less than 0, which meets the requirement of the chemical reaction evolution. This result can realize the relatively sharp formation of $Cd(Im)_2$ metal-organic framework at optimum temperature. In addition, during prolonged reaction times, it is necessary to maintain the correct temperature to ensure that the desired material is obtained.

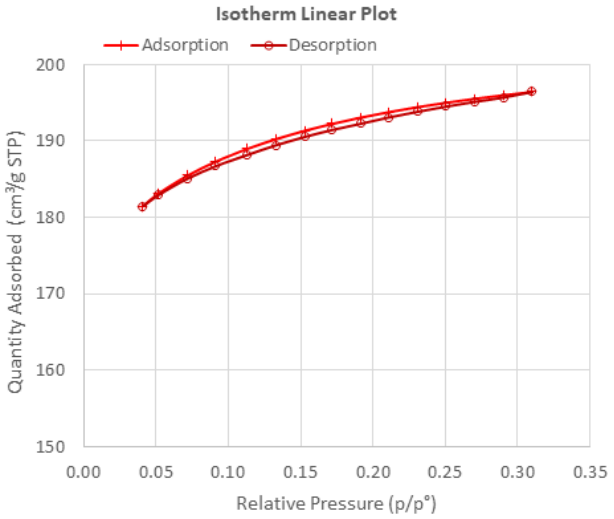

Figure 4: Isotherm linear plot of the $Cd(Im)_2$ at 150 °C

The porous property of $Cd(Im)_2$ was identified by measurement of surface area (BET) which was investigated using N_2 adsorption-desorption isotherms. Nitrogen adsorption isotherms show type I curves, which reveal the microporous nature. The BET surface area of $Cd(Im)_2$ in Figure 2c was 662.894 m^2/g or 858.389 m^2/g with Langmuir surface area (Figure 4). With this characteristic, $Cd(Im)_2$ can adsorb various objects, such as gases, vapors, toxic organic compounds, or heavy metal ions in water. This study tested the $Cd(Im)_2$ metal-organic framework for the adsorption of the chromogenic organic compound Rhodamine B in an aqueous medium.

Rhodamine B adsorption onto the of Cd-ZIF-8

The adsorption capacity of RhB in solution on $Cd(Im)_2$ was investigated. The results of determining the adsorption capacity according to the initial concentration are presented in Table 1 below. Freundlich's and Langmuir's adsorption models were applied to evaluate and calculate the maximum adsorption capacity. According to the Langmuir model, the maximum adsorption capacity of Cd-ZIF-8 for RhB was recorded at 64.52 $mg.g^{-1}$.

Table 1: The RhB adsorption capacity of Cd-ZIF-8

C_0 (mg/L)	19.276	39.831	59.165	78.321	99.986
C_e (mg/L)	0.043	0.183	1.830	16.890	35.486
q_e (mg/g)	19.233	39.648	57.336	61.432	64.500
C_e/q_e	0.002	0.005	0.032	0.275	0.550

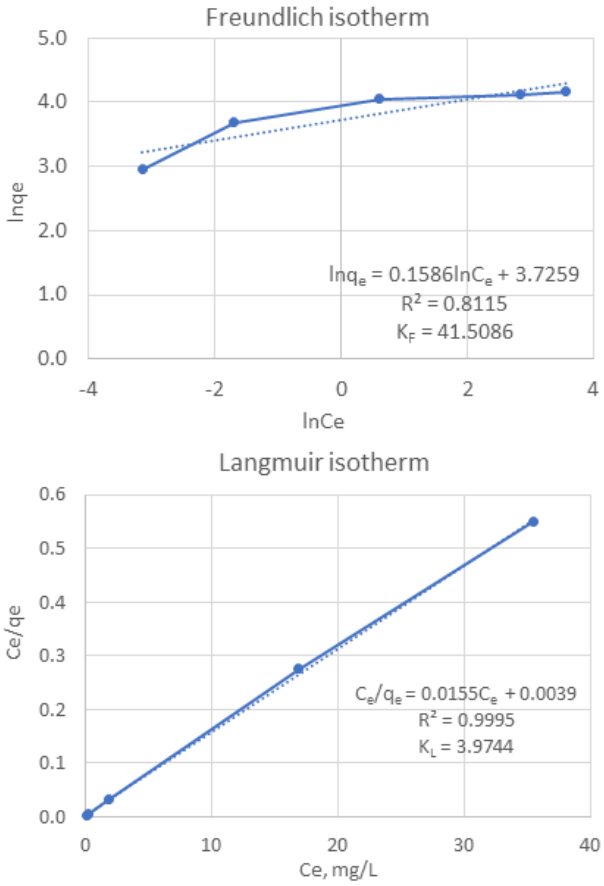

Figure 5: The maximum adsorption capacity of Cd-ZIF-8 for RhB

Table 2: Parameters and correlation coefficients for isotherms and kinetic models of Cd-ZIF-8 adsorption

Pseudo-first-order model			Pseudo-second-order model		
k_1 (min^{-1})		R^2	k_2 ($g.mg^{-1}.min^{-1}$)		R^2
0.030169		0.8839	0.00024		0.9472
Langmuir isotherm			Freundlich isotherm		
q_{max} (mg/g)	K_L (L/mg)	R^2	K_F	n	R^2
64.52	41.509	0.9995	41.509	6.3052	0.8115

https://doi.org/10.51316/jca.2023.033

A critical factor in determining the efficiency of an adsorption process is knowing the suitable time of contact between an adsorbate and the adsorbent that allows maximum adsorption. The effect of different initial contact times was investigated, and the result is shown in table 2. The adsorption data of Cd-ZIF-8 were well fitted with a pseudo-second-order model at R^2 = 0.9472 (Figure 6). It suggested that the rate-limiting step in the adsorption process might be chemisorption [24].

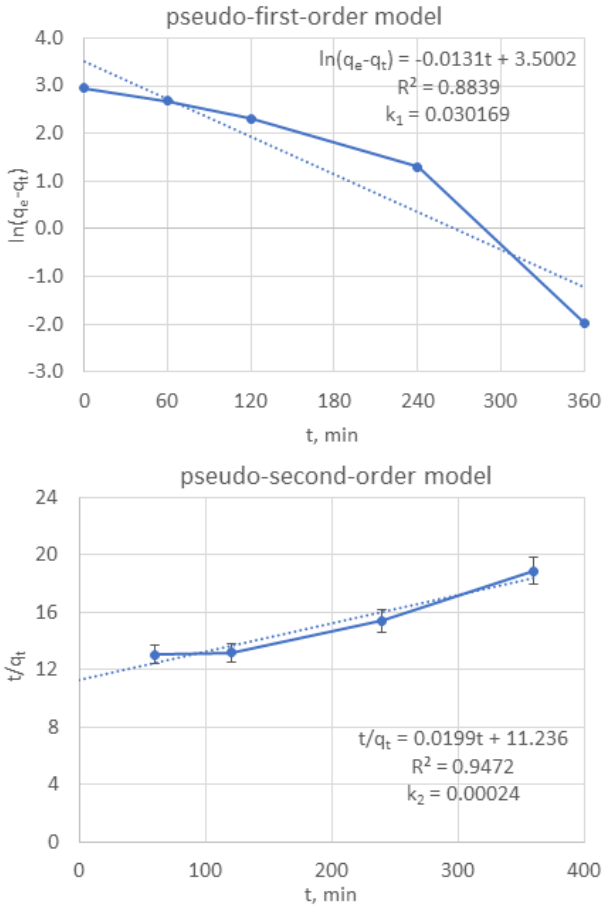

Figure 6: The kinetic models of Cd-ZIF-8 adsorption

The adsorption of Rhodamine B onto the Cd-ZIF-8 fitted well with Langmuir and Freundlich isotherm models (Figure 5), which confirms the surface adsorption sites on adsorbents were of homogeneous distribution, and the adsorption of Rhodamine B on the Cd-ZIF-8 material might occur in the monolayer model.

Reusability of the Cd-ZIF-8

To make the adsorption process cost-effectively, a adsorbent should have a high recycling ability, which could open the way to pilot-scale applications. Herein, we also investigated whether prepared Cd-ZIF-8 could regenerate its adsorption sites by performing five adsorption/desorption cycles. Regeneration cycles are displayed in Figure 6, where we can see the RhB removal percentage dropping slightly after five runs of the adsorption/desorption process. After the first cycle, which shows the highest value (99.78%), a slight decrease in RhB regeneration can be observed. It reaches 92.03% in the fifth cycle, which can be due to a reduction of available sites for adsorption. The negligible decrease in removal percentage after five cycles indicates the excellent applicability of the prepared Cd-ZIF-8 for dye removal in practice.

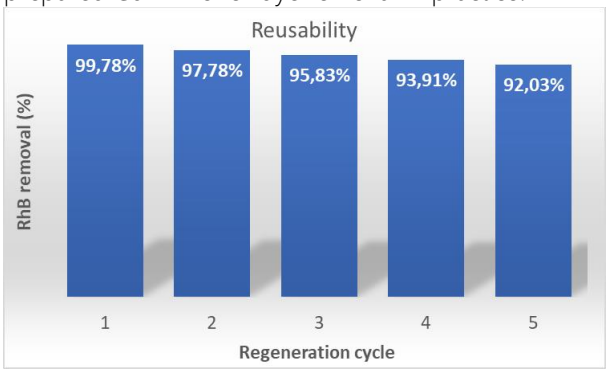

Figure 7: Recycling performance of Cd-ZIF-8 in the removal of RhB.

Conclusion

The present study explored the successful use of a synthesized cadmium zeolitic-imidazolate framework (Cd-ZIF-8) for the adsorption and removal of Rhodamine B from an aqueous solution at different operating conditions. XRD, BET, FT-IR, and SEM techniques characterized and confirmed the prepared material. The BET surface area of Cd(Im)2 was 662.894 m2/g, while SEM analysis showed micrometer-sized crystals with uniform network fibers. The Langmuir isotherm was found to fit more satisfactorily than the Freundlich isotherm, the favorable adsorption of RhB onto the adsorbent. The corresponding maximum adsorption capacity was equal to 64.52 mg/g. The obtained thermodynamic parameters indicated an endothermic adsorption process; thus, raising the temperature led to more significant RhB adsorption. The kinetic study showed that RhB adsorption on Cd-ZIF-8 followed a pseudo-second-order model, suggesting that the dominant adsorption mechanism is chemisorption. The adsorption-desorption efficiency of the Cd-ZIF-8 was examined for up to five successive cycles and showed excellent reusability performance. Based on the results of the present work, the proposed material could be considered an excellent adsorbent for effective dye removal, opening new paths for further research.

https://doi.org/10.51316/jca.2023.033

Acknowledgments

This research is funded by Institute of Chemistry and Materials under a grant the Basic project for Young scientists.

References

1. T.A. Khattab, M.S. Abdelrahman, M. Rehan, Envir. Sci. Pol. R 27 (2019) 3803-3818. https://10.1007/s11356-019-07137-z
2. M.A. Hassaan, A.E. Nemr, Ame. Jou. Env. Sci. Eng 1(3) (2017) 64-67. https://10.11648/j.ajese.20170103.11
3. M. Gavrilescu, Water, 13(19) (2021) 2746. https://doi.org/10.3390/w13192746
4. Francesco Testa, T.D., Maria Rosa De Giacomo, Fabio Iraldo, Marco Frey, Jou. Cle. P 64 (2014) 91-97. https://doi.org/10.1016/j.jclepro.2013.08.003
5. V.H. Nguyen, D.T. Nguyen, T.T. Nguyen, H.P.T. Nguyen, H.B. Khuat, T.H. Nguyen, V.K. Tran, S.W. Chang, P.N. Tri, D.D. Nguyen, D.D. La, Env. Tec. I 24 (2021) 101811. https://doi.org/10.1016/j.eti.2021.101811
6. K.S. Park, Z. Ni, A.P. Côté, O.M. Yaghi, T. Pro. Nat. Aca. Sci (PNAS) 103(27) (2006) 10186-10191. https://doi.org/10.1073/pnas.0602439103
7. Surendra Sasi Kumar Jampa, A.P.U., Rajesh Vanshpati, Sivakumar Pandian, Manish Kumar Sinha, Swapnil Dharaskar, Env. Tec. I (2020) 19.
8. S. Wongprakarn, J. Prasongkit, P. Srepusharawoot, Jap . Jou. App. P 53 (2014) 08NK03. http://dx.doi.org/10.7567/JJAP.53.08NK03
9. Y. Liu, H. Cheng, M. Cheng, Z. Liu, D. Huang, G. Zhang, B. Shao, Q. Liang, S. Luo, T. Wu, S. Xiao, Che. Eng. J 417 (2021) 127914. https://doi.org/10.1016/j.cej.2020.127914
10. J.O. Ighalo, S. Rangabhashiyam, C.A. Adeyanju, S. Ogunniyi, A.G. Adeniyi, C.A. Igwegbe, Jou. Ind. Eng. C 105 (2022) 34-48. https://doi.org/10.1016/j.jiec.2021.09.029
11. K. Ahmad, H.R. Shah, M. Ashfaq, S.S.A. Shah, E. Hussain, H.A. Naseem, S. Parveen, A. Ayub, Foo. Che. T 149 (2021) 112008. https://doi.org/10.1016/j.fct.2021.112008
12. B.B. Mohammed, H. Lgaz, A.A. Alrashdi, K. Yamni, N. Tijani, Y. Dehmani, H.E. Hamdani, I.M. Chung, Ara. Jou. C 14 (2021) 102897. https://doi.org/10.1016/j.arabjc.2020.11.003
13. M. Mohsen, I. Naeem, M. Awaad, H. Tantawy, A. Baraka, Jou. Sol. Sta. C 289 (2020) 121493. https://doi.org/10.1016/j.jssc.2020.121493
14. M. Chin, C. Cisneros, S.M. Araiza, K.M. Vargas, K.M. Ishihara, F. Tian, RSC A 8 (2018) 26987. https://10.1039/C8RA03459A
15. S. Yuan, S. Yun, Y. Zhang, J. Dang, M. Sun, C. Dang, Y. Deng, Jou. Mat. Che. C 9(40) (2021) 14408-14420. https://doi.org/10.1039/D1TC02734D
16. Y. Feng, Y. Li, M. Xu, S. Liu, J. Yao, RSC A 6(111) (2016) 109608-109612. https://doi.org/10.1039/C6RA23870J
17. V.A. Tran, K.B. Vu, T.T.T. Vo, V.T. Le, H.H. Do, L.G. Bach, S.W. Lee, App. Sur. S 538 (2021) 148065. https://doi.org/10.1016/j.apsusc.2020.148065
18. V.A. Tran, A.N. Kadam., S.W. Lee, Jou. All. C 835 (2020) 155414. https://doi.org/10.1016/j.jallcom.2020.155414
19. R. Lamari, B. Benotmane, F. Mostefa, Ira. Jou. Che. Che. E 41(6) (2022) 1985-1999. https://10.30492/IJCCE.2021.131068.4236
20. A. Karami, R. Shomal, R. Sabouni, M.H. Al-Sayah, A. Aidan, Ene 15(13) (2022) 4642. https://doi.org/10.3390/en15134642
21. S.A. Sadat, A.M. Ghaedi, M. Panahimehr, M.M. Baneshi, A. Vafaei, M. Ansarizadeh, App. Sur. S 467-468 (2019) 1204-1212. https://doi.org/10.1016/j.apsusc.2018.10.274
22. Y.T. Li, S.Y. Yao., Y. Wang, K.H. Cui, C.J. Jiang, Y.Q. Tian, Cry. Eng. C 13(10) (2011) 3470-3473. https://doi.org/10.1039/C1CE05055A
23. L. Li, B.B. Guo, G. Li, Ino. Che. C 35 (2013) 351-354. https://dx.doi.org/10.1016/j.inoche.2013.06.046
24. H. Guo, F. Lin, J. Chen, F. Li, W. Weng, App. Org. C 29(1) (2014) 12-19. https://doi.org/10.1002/aoc.3237